Taylor & Francis
Taylor & Francis Group

Artificial Cells, Nanomedicine, and Biotechnology

An International Journal

ISSN: 2169-1401 (Print) 2169-141X (Online) Journal homepage: informahealthcare.com/journals/ianb20

Microneedle-mediated transdermal delivery of nanostructured lipid carriers for alkaloids from *Aconitum sinomontanum*

Teng Guo, Yongtai Zhang, Zhe Li, Jihui Zhao & Nianping Feng

To cite this article: Teng Guo, Yongtai Zhang, Zhe Li, Jihui Zhao & Nianping Feng (2018) Microneedle-mediated transdermal delivery of nanostructured lipid carriers for alkaloids from *Aconitum sinomontanum*, Artificial Cells, Nanomedicine, and Biotechnology, 46:8, 1541-1551, DOI: 10.1080/21691401.2017.1376676

To link to this article: https://doi.org/10.1080/21691401.2017.1376676

ARTIFICIAL CELLS, NANOMEDICINE, AND BIOTECHNOLOGY
2018, VOL. 46, NO. 8, 1541–1551
https://doi.org/10.1080/21691401.2017.1376676

Microneedle-mediated transdermal delivery of nanostructured lipid carriers for alkaloids from *Aconitum sinomontanum*

Teng Guo, Yongtai Zhang, Zhe Li, Jihui Zhao and Nianping Feng

Department of Pharmaceutical Sciences, School of Pharmacy, Shanghai University of Traditional Chinese Medicine, Shanghai, PR China

ABSTRACT

A combination method using microneedle (MN) pretreatment and nanostructured lipid carriers (NLCs) was developed to improve the transdermal delivery of therapeutics. The MN treatment of the skin and co-administration of NLCs loaded with total alkaloids isolated from *Aconitum sinomontanum* (AAS–NLCs) significantly increased the skin permeation of the drugs. Fluorescence imaging confirmed that MNs could provide microchannels penetrating the stratum corneum, and delivery of NLCs through the channels led to their deeper permeation. *In vivo* studies showed that combination of AAS–NLCs with MNs (AAS–NLCs–MN) in transdermal delivery could improve the bioavailability and maintain stable drug concentrations in the blood. Moreover, AAS–NLCs–MN showed benefits in eliminating paw swelling, decreasing inflammation and pain, and regulating immune function in adjuvant arthritis rats. After administration of AAS–NLCs–MN, no skin irritation was observed in rabbits, and electrocardiograms of rats showed improved arrhythmia. These results indicated that the dual approach combining MN insertion and NLCs has the potential to provide safe transdermal delivery and to improve the therapeutic efficacy through sustained release of AAS.

ARTICLE HISTORY
Received 28 August 2017
Revised 2 September 2017
Accepted 2 September 2017

KEYWORDS
Nanostructured lipid carriers; microneedle; transdermal delivery; anti-inflammatory and analgesic effects; cardiotoxicity

Introduction

As a non-invasive route, transdermal drug delivery is one of the most important alternatives to parenteral administration. However, the largest challenge in percutaneous administration is to penetrate the stratum corneum (SC) barrier and maintain the skin integrity at the same time [1]. The use of a microneedle (MN) array is an efficient physical penetration enhancement technique, which disrupts the SC barrier by creating multiple microchannels without damaging the skin, enhances drug transdermal transport [2,3]. Meanwhile, lipid-based particulate carriers are another approach to enhancing the skin permeation of drugs. As a second generation of lipid nanoparticle-based drug vehicles, nanostructured lipid carriers (NLCs) have attracted broad interest for transdermal drug delivery because of their capability of film formation, skin hydration, and controlled occlusion [4,5]. At room temperature, the structure of NLCs contains both solid and liquid lipids, which provide better protection for loaded actives and enhance the percutaneous permeation [6].

Aconitum sinomontanum Nakai contains several diterpenoid alkaloids, which show strong analgesic and anti-inflammatory effects [7]. In a previous study, NLCs have been designed and optimized for percutaneous administration of alkaloids isolated from *A. sinomontanum* (AAS) [8]. However, the results obtained indicated that nanoparticle integrity during transdermal delivery was consistent with that of lipid nanoparticles, which are not considered to penetrate SC [9]. Without the use of physical methods enhancing skin permeation, nanoparticles follow passive routes of permeation through hair follicles, and the efficiency of drug penetration is greatly restricted. To address this problem, MN-mediated delivery was developed, and the technology has been used to enhance the skin permeation of various nanocarriers [10]. Since they combine physical and chemical osmosis, MNs can transiently break the barrier properties of the skin, while NLCs offer a wide range of benefits, including enhanced hydration and prolonged release into the skin, protection of actives, and decreased skin irritation. To date, most studies of MN-mediated delivery of nanocarriers have been aimed at achieving transdermal delivery of vaccines, dyes, and compounds [11–13].

In the present study, the *in vitro/in vivo* transdermal characteristics of AAS-loaded NLCs, combined with MN treatment (AAS–NLCs–MN), were investigated. To elucidate the transdermal delivery mechanism of AAS–NLCs–MN, the integrity of the nanoparticles during MN-assisted transdermal delivery was evaluated, and visualization of the transport of NLCs using MNs was performed. Moreover, the pharmacodynamics, skin irritation, and cardiac toxicity were also investigated after percutaneous administration of AAS–NLCs–MN.

Materials and methods

Materials

Microneedles with a 250-μm height, 100-μm width at the base, 300-μm interspacing, and 5×5 mm area were

CONTACT Nianping Feng npfeng@hotmail.com, npfeng@shutcm.edu.cn Department of Pharmaceutical Sciences, School of Pharmacy, Shanghai University of Traditional Chinese Medicine, 1200 Cailun Road, Shanghai 201203, PR China

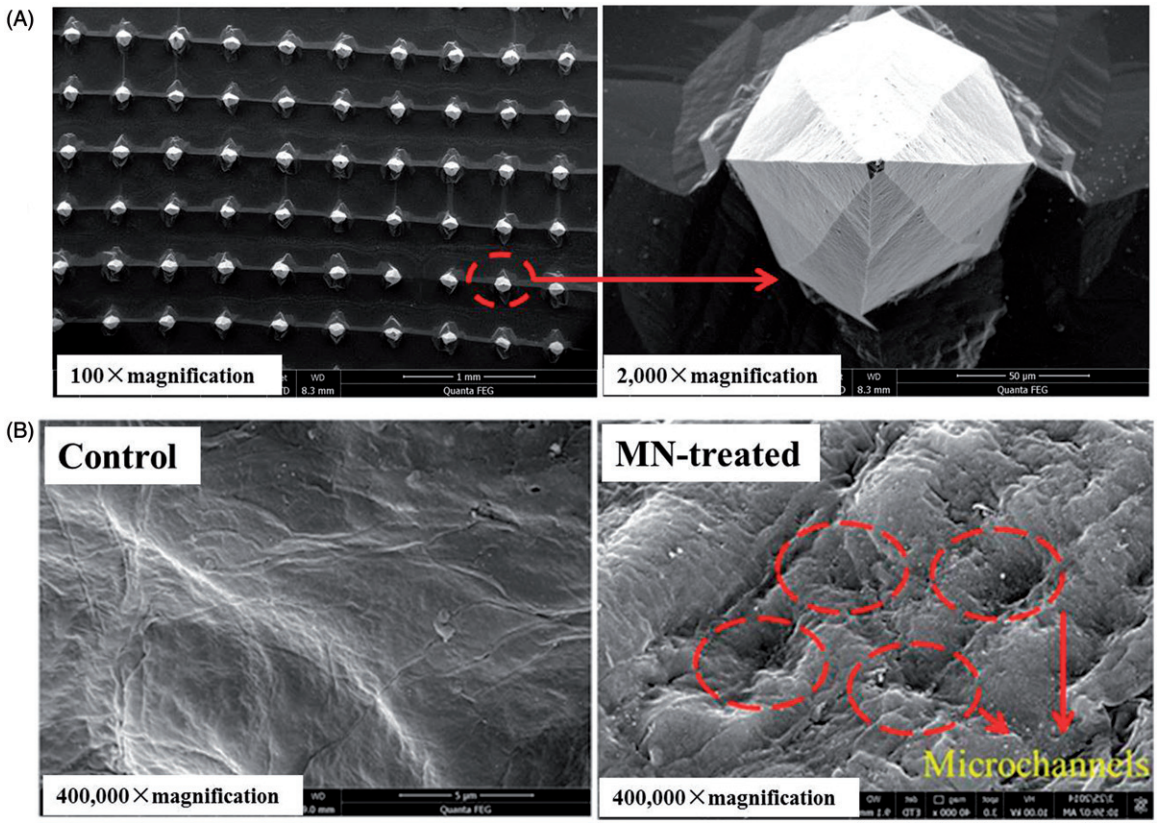

Figure 1. SEM images of (A) microneedles and (B) skin from the control and MN-treated nude mice.

purchased from Jiangsu Natong Biological Co., Ltd. (Suzhou, China). A scanning electron microphotograph of MNs is shown in Figure 1(A). Lappaconitine (LA) and ranaconitine (RAN) (purity >98% each) were purchased from Shaanxi Chenguang Pharmaceutical Co., Ltd. (Xi'an, China). Enzyme-linked immunosorbent assay (ELISA) kits for interleukin (IL)-1β, IL-6, tumour necrosis factor alpha (TNFα), beta-endorphin (β-EP), and Substance P (SP), as well as a colorimetric kit for nitric oxide (NO), were purchased from Shanghai Xitang Biological Co., Ltd. (Shanghai, China). All other chemicals were of high-performance liquid chromatography (HPLC) or analytical grade.

Animals

Male Sprague–Dawley rats, nude mice, and New Zealand White rabbits, weighing 200 ± 20 g, 25 ± 5 g, and 2.0–2.5 kg, respectively, were used in this study. The animal experiments were conducted with the approval of the Animal Ethical Committee of Shanghai University of Traditional Chinese Medicine (permit SYXK [Hu] 2009-0069).

Effect of microneedle treatment on SC structure

A nude mouse was anesthetized and immobilized with the abdomen facing upward, and then the skin in the abdomen region was divided into two areas. An MN array was fixed to an applicator (Nantong Biological Co., Ltd., Nantong, China), which provided an insertion force of approximately 5 N. The insertion of MNs into the skin lasted for 3 min, and the MN-untreated skin area was maintained as a control region. The mouse was immediately euthanized, and the abdominal skin was collected and washed with normal saline. The skin samples were fixed in glutaraldehyde for 24 h, rinsed with phosphate-buffered saline (PBS, pH 7.4), fixed in 1% osmic acid, dehydrated with ethanol, and then dried using CO_2 critical point drying. Finally, the skin was sputtered with platinum and evaluated using a scanning electron microscope (SEM; Quanta FEG250; FEI, Hillsboro, OR, USA).

In vitro *permeation studies*

Extraction of AAS and preparation of AAS–NLCs were conducted according to previous methods [8]. The main components of AAS, which have superior pharmacological effects, were LA and RAN (yield: 69.47% and 9.16%, w/w, respectively). AAS–NLCs were successfully prepared with the following components in optimal proportions: Precirol ATO5, Labrasol®, Cremophor RH40, and AAS (6.7%, 2.3%, 5.5%, and 0.9%, w/v, respectively). Rats were anesthetized and euthanized, their abdominal fur was removed with a razor, and then the skin was carefully excised and washed with normal saline. MN arrays were continuously applied in the centre of the skin at a force of 5 N for 3 min, and MN-untreated skin samples were prepared as control samples. *In vitro* permeation experiments were conducted with the MN-treated and MN-untreated skin samples fit into a Franz diffusion cell (Fulansi Electronic Science and Trade Co, Ltd., Tianjin, China). Each donor compartment had a diffusion area of 2.0 cm^2, and 1 ml of test formulations was added to the compartment.

To provide sink conditions, each receptor compartment was filled with 12.5 ml of freshly prepared normal saline containing 20% polyethylene glycol 400 (v/v), which was magnetically stirred (500 rpm) and maintained at 37 ± 0.5 °C [14]. At predetermined time points, 1 ml of the sample was removed from the receptor compartment and replaced with an equal volume of the receptor fluid equilibrated to 37 ± 0.5 °C. The concentrations of LA and RAN in the collected samples were analysed using HPLC under the following conditions: an Agilent HPLC system (HP 1260; Agilent Technologies, Inc., Santa Clara, CA, USA) coupled with an Inspire™ C18 column (250 mm × 4.6 mm, 5 μm; Dikma Technologies, Beijing, China), with a mobile phase consisting of methanol and a 0.01 mol/l monosodium phosphate aqueous solution (80:20, v/v), and a flow rate of 1.0 ml/min. The column temperature was maintained at 30 °C, and the detection wavelength was 252 nm.

Fluorescence detection-based nanoparticle tracking analysis (NTA) in receptor fluid

A Franz diffusion cell with the MN-treated rat skin fit was prepared as described earlier. The donor compartment was filled with 1.0 ml of NLC formulations containing 10 μg/mL coumarin-6 (C6), and the receptor compartment was filled with PBS (pH 7.4) containing 0.02% sodium azide. After 12 h, the receptor fluid was removed, and the fluorescence was measured using a NanoSight NS300 system (Malvern Instruments, Malvern, UK), a 405-nm laser with a temperature control, and a 503-nm long-pass filter for fluorescent particle analysis. The temperature was maintained at 25 °C throughout the experiment, and the NanoSight NS300 NTA 3.0 software was used for data collection.

Visualization of NLC transport upon using MNs

Microneedle-untreated and MN-treated skin samples of nude mice were acquired as described above and carefully sandwiched in a Franz diffusion cell. PBS (pH 7.4) containing 0.02% NaN_3 was used as the receptor fluid, and 1 ml of each NLC formulation containing 10 μg/mL C6 was added to the donor compartment of the MN-untreated and MN-treated skin samples, while 1 ml of a physical mixture of C6 (10 μg/mL) and blank NLCs was added to the donor compartment of an MN-treated skin sample. The diffusion cell was stirred at 500 rpm, and the temperature was maintained at 37 ± 0.5 °C. After 6 h, the skin was removed, and the excess preparations were carefully wiped out from the surface of the skin. The skin sample was cut into squares of 0.5 × 0.5 cm, which were put onto microscopic slides. The full skin thickness was optically scanned through the Z-axis of a Zeiss LSM 710 microscope (Carl Zeiss, Thornwood, NY, USA).

In vivo *bioavailability*

Rats were anesthetized with an intraperitoneal injection of a urethane aqueous solution (1.3 g/kg), and their abdominal fur was removed with a razor. The experiments were conducted with the following six groups of rats ($n = 5$ each): (1) 0.3 or 1 ml of NLC formulations was subcutaneously injected into the abdominal skin; (2) patches containing 0.3 or 1 ml of NLCs were applied to the abdominal skin and fixed with a tape; (3) MNs were applied at a force of 5 N for 3 min to the abdominal skin, and patches containing 0.3 or 1 ml of NLCs were applied to the same application sites.

In all the groups, blood samples were collected from the ocular vein for 48 h and then centrifuged at 5000 rpm for 10 min. A volume of 100 μL of plasma was withdrawn from each supernatant, and 600 μL of acetonitrile was added to each plasma sample. After mixing for 5 min with a vortex mixer and centrifugation at 12,000 rpm for 10 min, the organic solvent layer was collected from each plasma sample, dried under a gentle nitrogen gas stream, and dissolved in methanol. Plasma drug concentrations were analysed using a triple-quadrupole ultra-performance liquid chromatography–tandem mass spectrometry system (Thermo Finnigan, San Jose, CA, USA). The experiment was performed with a Hypersil GOLD™ C18 column (100 mm × 2.1 mm, 5 μm; Thermo Finnigan, San Jose, CA, USA). The mobile phase consisted of methanol:water:acetic acid (70:30:0.2, v/v/v), and a flow rate was 0.2 ml/min. The precursor-to-production transitions were monitored at *m/z* 5 8 5 → 356 for LA and *m/z* 6 0 1 → 422 for RAN using a selected reaction monitoring mode.

Pharmacodynamic study

Adjuvant arthritis induction and treatment

To induce adjuvant arthritis (AA), rats were injected intradermally with 0.2 ml of Freund's complete adjuvant (FCA; Sigma-Aldrich, St. Louis, MO, USA) into the left hind metatarsal footpad [15]. After seven days, all rats were divided into five groups ($n = 8$) as follows: a normal group, AA model group, AAS–NLCs (1.5 ml/kg, daily) subcutaneous injection group, AAS–NLCs (5 ml/kg, daily) patch group, and MN-treated/AAS–NLCs (5 ml/kg, daily) patch group. From day 1 to day 14 after the adjuvant induction, the normal and AA model rats were treated with the normal saline, and the remaining three groups were treated using the different drug deliveries of AAS–NLCs. The paw volume was measured using a plethysmometre (Yiyan Electronic Science Co., Ltd., Jinan, China).

Histological analysis

On day 14 after the adjuvant induction, the hind paws were excised, fixed in 10% neutral buffered formalin for 72 h, and decalcified with 10% ethylenediaminetetraacetic acid for 30 days. Tissues were sectioned, embedded in paraffin, and stained with haematoxylin and eosin (HE). Slides were viewed under an optical microscope (BH-2; Olympus, Tokyo, Japan) for histopathological changes.

Organ index assay

At the end of the arthritis observation period (14 days), the rats were euthanized. The heart, spleen, thymus, and kidneys were promptly removed and weighed. The organ index was calculated as the ratio of the organ wet weight to the body weight (mg/g, respectively) [16].

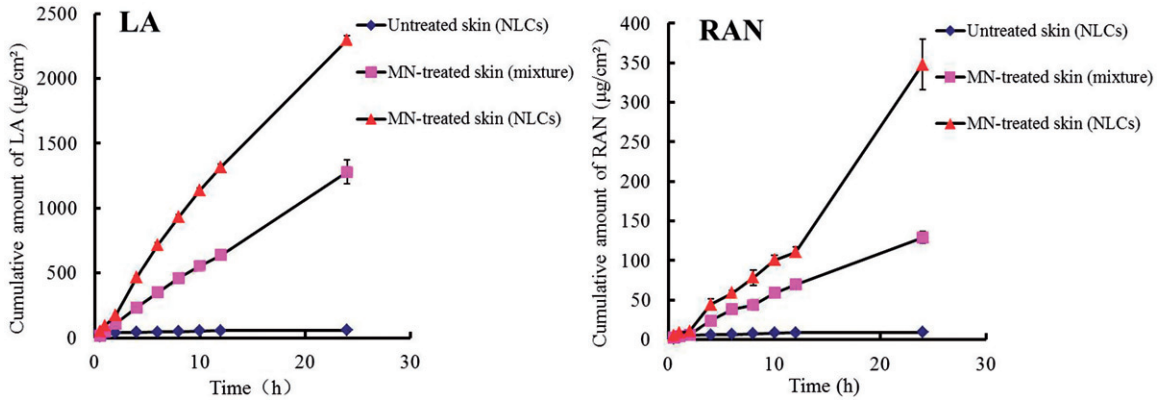

Figure 2. *In vitro* skin permeation profiles of LA and RAN from AAS–NLCs and a physical mixture of AAS and blank NLCs applied to the MN-treated skin and AAS–NLCs applied to the untreated skin ($n = 3$).

Anti-inflammatory and analgesic effects

Blood was collected and allowed to clot for 30 min, and the serum was obtained by centrifugation at 3000 rpm for 10 min. Concentrations of IL-1β, IL-6, TNFα, β-EP, and SP were quantified in the serum by ELISA, and serum NO concentrations were determined by a colorimetric assay, according to the manufacturer's protocols. All assays were conducted in a blinded fashion.

Skin irritation

The hair on the back of rabbits was shaved, and the animals were divided into three groups: in two groups, NLCs (1.0 ml), with or without AAS, were applied to an area of 3×3 cm, and in the third group, MNs were applied at a force of 5 N for 3 min with 1.0 ml of AAS–NLCs. After 4 h, the formulations were removed by gentle washing, and then the skin was inspected for an erythema and/or oedema. The experimental formulations were tested once a day for three consecutive days, and skin irritation was examined at 24, 48, and 72 h after the treatment. Finally, the rabbits were euthanized, and the tested skin regions were removed, fixed in 10% neutral buffered formalin for 72 h, and embedded in paraffin. Serial paraffin sections were stained with HE and viewed under an optical microscope.

Cardiotoxicity

Rats were anesthetized and immobilized with the abdomen facing upward. The abdominal fur was removed, and the rats were divided into five groups: a blank group, AAS–NLCs (1.5 ml/kg) subcutaneous injection group, AAS–NLCs (5 ml/kg) patch group, MN-treated/AAS–NLCs (5 ml/kg) patch group, and MN-treated/patch group treated with a mixture of AAS and blank NLCs (5 ml/kg). After 30 min, electrocardiograms (ECGs) were recorded with a DASA 4600 multi-channel physiology recorder (Gould Corp., NY, USA). ECG signals were recorded from each rat for a total duration of 30 min.

Statistical analysis

Results are presented as the mean ± standard deviation. Differences were analysed using the Student's *t*-test with the Statistical Program for Social Sciences software version 19.0 (IBM Corp., Armonk, NY, USA). $p < .05$ were considered statistically significant. The pharmacokinetic parameters of LA and RAN were calculated using non-compartmental analysis with the DAS 2.0 software (Mathematical Pharmacology Professional Committee of China, Shanghai, China).

Results and discussion

Effect of microneedle treatment on the SC structure

As shown in Figure 1(B), the surface of the control nude mouse skin (without any treatment) was intact and smooth. However, the image acquired after the insertion of MNs into the nude mouse skin showed the evidence of penetration as representative pores created by the MN array in the treated area, which indicated that MNs were inserted into the skin to create microchannels for transdermal transport.

In vitro *permeation studies*

The *in vitro* skin permeability for particles increases by orders of magnitude upon using MNs [12]. In our study, MN treatment effectively enhanced the transdermal penetration of LA and RAN contained in an AAS–NLC preparation compared to that observed in the MN-untreated group (Figure 2). The enhancement of transdermal drug delivery may be attributed to the ability of MNs to disrupt the barrier function of SC in a minimally invasive fashion. Moreover, under the same MN treatment conditions, the AAS–NLC formulations significantly enhanced the *in vitro* AAS percutaneous permeation compared to that shown by a physical mixture of AAS and NLCs. The results showed that the cumulative amounts of NLC-associated LA and RAN that penetrated the rat skin *in vitro* were $2{,}296.27 \pm 33.98$ and 347.79 ± 31.64 μg/cm^2, while those from the physical mixture were $1{,}280.15 \pm 90.32$ and 128.91 ± 7.50 μg/cm^2, respectively. This disparity is most likely due to higher solubility and better biocompatibility with the skin of the drugs in the nanoparticle formulation [17]. The AAS-loaded NLCs combined with MNs achieved higher *in vitro* percutaneous permeation than that observed with the other drug delivery modes.

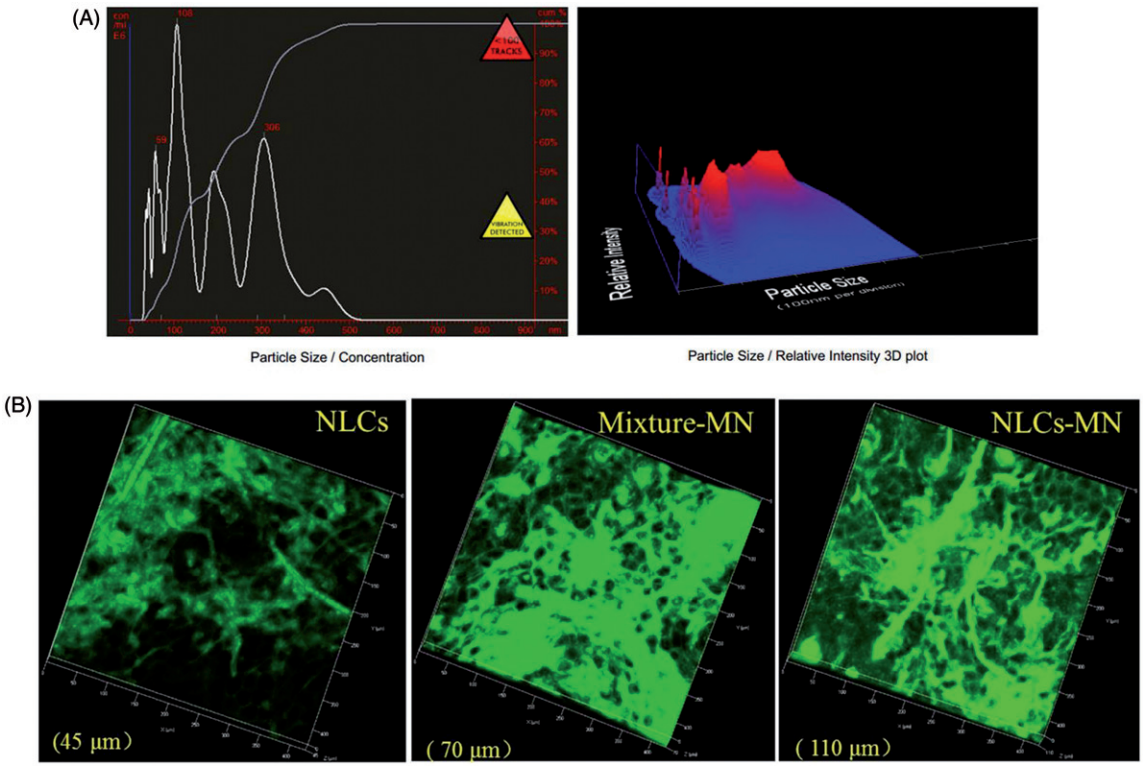

Figure 3. Analysis of NLC transport upon using MNs. (A) NanoSight image of a skin sample treated with MNs and C6-NLCs, (B) laser scanning confocal microscopy images of an untreated nude mouse skin after administration of C6-NLCs (NLCs), MN-treated skin after application of a mixture of C6 and blank NLCs (Mixture-MN), and MN-treated skin after application of C6-NLCs (NLCs-MN).

NTA

A previous study has revealed that C6-labeled NLCs do not penetrate SC in their intact form [8]. However, some C6-labeled nanoparticles were detected by fluorescence detection-based NTA after NLCs were applied to the MN-treated rat skin (Figure 3(A)), demonstrating that MNs could increase the skin permeability for nanoparticles. This finding is consistent with reports that detected nanoparticles crossing the skin, which suggests the possibility of using MNs to deliver controlled release particles [18].

Visualization of NLC transport upon using MNs

The differences in skin permeation of C6 were confirmed by confocal microscopy images taken in the Z direction, which is defined as perpendicular to the skin surface [19]. As shown in Figure 3(B), visualization of the depth of penetration into MN-treated skin samples incubated with NLCs demonstrated relatively deep C6 permeation, with green fluorescence detectable at a depth of 110 μm. In comparison, the diffusion depth for MN-untreated skin samples was approximately 45 μm, suggesting that nanoparticles could not penetrate the SC barrier without MN treatment but could passively permeate into the skin via the follicular pathway [20]. Meanwhile, MNs could create microchannels penetrating SC to deliver the fluorescent dye through the channel to achieve deeper C6 permeation. On the other hand, the fluorescence in the MN-treated skin samples incubated with the physical mixture of NLCs and C6 almost disappeared at a depth of 70 μm, which showed lower skin permeability of the mixture compared with that of C6-NLCs. The deeper skin penetration upon MN-NLC delivery may be attributed to the ability of C6 released from these NLCs to freely diffuse laterally, as indicated by the fluorescence around microchannels and in deeper skin layers, allowing the accelerated transdermal delivery of the dye [2,21]. Furthermore, in agreement with the results of the *in vitro* permeation experiments, the fluorescence intensity obviously increased for the perforated skin samples treated with C6-NLCs. In accordance with the physical ability of MNs and chemical ability of NLCs to enhance the skin penetration, the MN-mediated NLC delivery was able to effectively deliver the fluorescent dye through SC, which is beneficial for drug absorption into systemic circulation [10].

In vivo *bioavailability*

To assess the effect of drug delivery on the absorption rate of AAS into systemic circulation, 0.3 or 1 ml of AAS–NLCs was administered to rats by transdermal treatment with or without MNs. As shown in Figure 4, based on a high mortality rate of rats following hypodermic injection (i.h.) administration of 1 ml of AAS–NLCs (death rate was 100% after 1 h), the dose of subcutaneous injection was decreased accordingly. The plasma concentration–time curves of LA and RAN are depicted in Figure 4, and the results for some pharmacokinetic parameters are summarized in Tables 1 and 2. The peak concentration (C_{max}) for the AAS–NLC formulation was the highest (LA and RAN, 97.26 ± 29.18 and 18.91 ± 2.70 ng/mL, respectively) at approximately 0.5 h after subcutaneous injection, suggesting rapid absorption and elimination of the drugs. This finding is consistent with that of a report showing

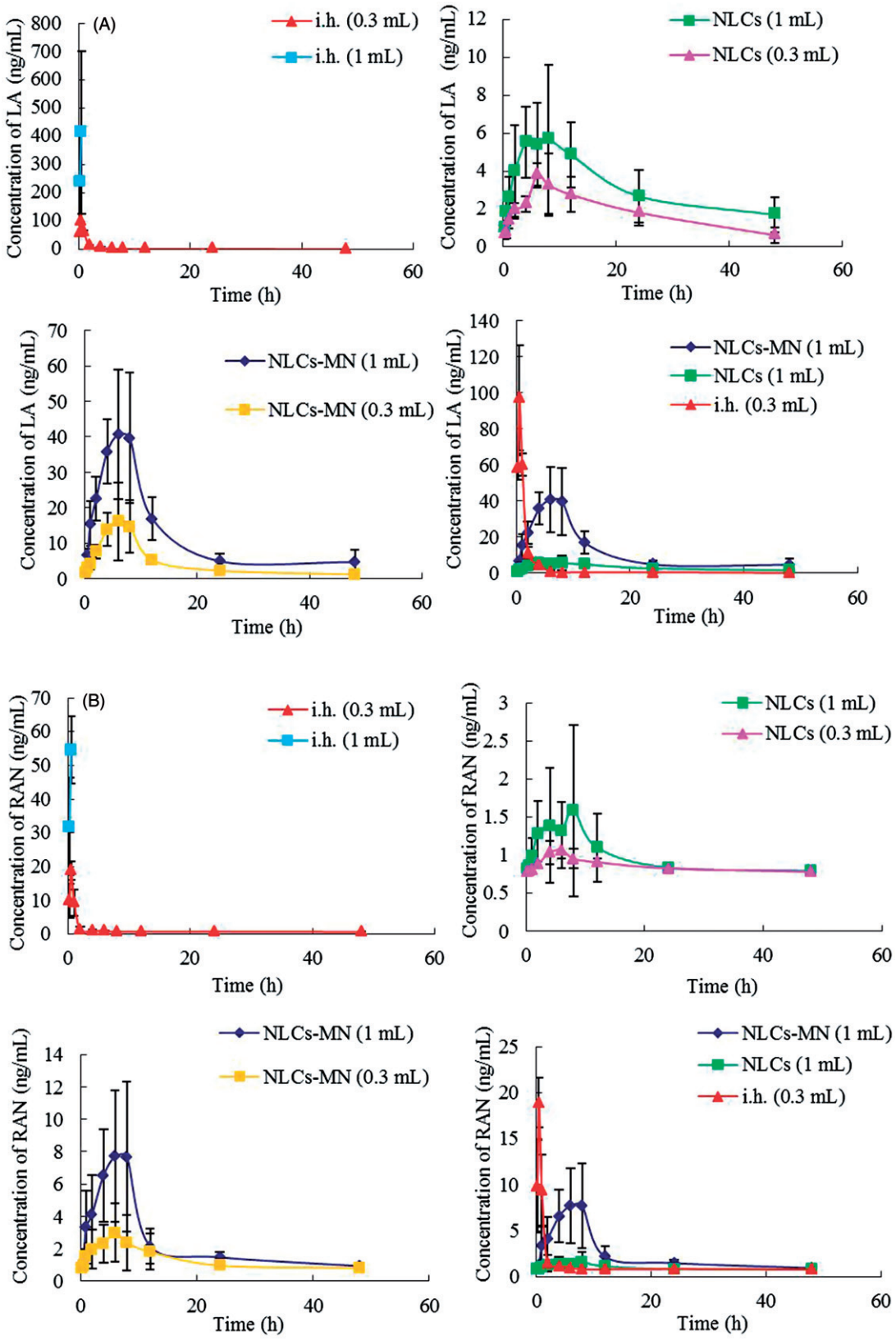

Figure 4. Representative mean plasma concentration–time profiles of (A) LA and (B) RAN after percutaneous and hypodermic applications ($n = 5$).

that alkaloid extracts of *A. sinomontanum* have a relatively short half-life [22]. The highest C_{max} values of LA and RAN could easily exceed the narrow therapeutic range and cause high mortality upon subcutaneous injection. In comparison, the C_{max} values of LA and RAN obtained after administering 1 ml of transdermal preparations were clearly reduced (MN-treated group: 47.00 ± 16.84 and 8.45 ± 4.86 ng/mL, respectively; MN-untreated group: 7.00 ± 2.81 and 2.14 ± 1.01 ng/mL,

Table 1. Pharmacokinetic parameters of LA released from AAS–NLCs in rats by transdermal treatment with or without microneedles and subcutaneous injection.

Parameter	i.h. (0.3 mL)	NLCs (0.3 mL)	NLCs (1 mL)	NLCs–MN (0.3 mL)	NLCs–MN (1 mL)
T_{max} (h)	0.50 ± 0.00	6.40 ± 0.89	6.00 ± 2.00	6.00 ± 2.00	6.00 ± 2.00
C_{max} (ng/mL)	97.26 ± 29.18	4.13 ± 1.18*	7.00 ± 2.81*	20.55 ± 9.22*,#	47.00 ± 16.84*,#
MRT_{0-t} (h)	3.58 ± 1.41	17.42 ± 2.23*	18.22 ± 2.47*	13.05 ± 1.83*	13.50 ± 1.89*
AUC_{0-t} (ng/mL × h)	139.62 ± 28.67	88.60 ± 23.74	154.94 ± 63.73	215.45 ± 43.47#	599.37 ± 192.58*,#

Mean ± SD, $n = 5$.
*$p < .05$ vs. i.h..
#$p < .05$ NLCs-MN vs. NLCs.

Table 2. Pharmacokinetic parameters of RAN released from AAS–NLCs in rats by transdermal treatment with or without microneedles and subcutaneous injection.

Parameter	i.h. (0.3 mL)	NLCs (0.3 mL)	NLCs (1 mL)	NLCs–MN (0.3 mL)	NLCs–MN (1 mL)
T_{max} (h)	0.50 ± 0.00	7.20 ± 3.03	5.20 ± 2.28	5.60 ± 0.89	5.60 ± 1.67
C_{max} (ng/mL)	18.91 ± 2.70	1.15 ± 0.18*	2.14 ± 1.01*	3.50 ± 1.59*,#	8.45 ± 4.86*,#
MRT_{0-t} (h)	16.77 ± 0.63	22.98 ± 0.41*	21.52 ± 1.67*	18.99 ± 2.46	15.52 ± 2.46
AUC_{0-t} (ng/mL × h)	55.92 ± 2.81	41.15 ± 1.25	46.89 ± 8.50	63.99 ± 21.70#	115.94 ± 40.26*,#

Mean ± SD, $n = 5$.
*$p < .05$ vs. i.h.
#$p < .05$ NLCs-MN vs. NLCs.

respectively) at approximately 6 h, indicating that transdermal delivery could reduce the drug toxicity by maintaining stable and lasting blood drug concentrations [23].

Moreover, the area under the concentration–time curve (AUC_{0-t}) values and the C_{max} values of LA and RAN were only slightly higher upon transdermal treatment without MNs and significantly increased with the increase in the nanocarrier dose upon MN-mediated delivery. MNs offer a method of increasing the transdermal drug absorption into systemic circulation by transiently compromising the barrier properties of SC [24]. The AUC_{0-t} values of LA and RAN released from 1 ml of AAS–NLCs after transdermal treatment with MNs were 3.9- and 2.5-fold higher, respectively, than those obtained without MNs ($p < .05$) and 4.3- and 2.1-fold higher, respectively, than those obtained after subcutaneous injection ($p < .05$). NLCs remained in the microchannels as drug reservoirs, which thereby enabled a controlled drug release. This is beneficial for the maintenance of short half-life drug concentrations in the plasma to achieve slower clearance and a higher AUC.

Pharmacodynamic study

Effects on paw swelling

The FCA-injected rats exhibited a significant increase in the volume of the injected paw compared with that in the normal control rats after the observation period. Administration of AAS–NLCs delivered by different modes significantly ($p < .05$) reduced the paw oedema compared with that in the arthritic group (Figure 5(A)). After treatment, the MN-treated/patch group showed the best inhibition of paw swelling, and the reduction of the paw oedema was more obvious in the patch group than that in the subcutaneous injection group. These results may be due to the fact that AAS–NLCs transdermal administered with MNs had the highest AUC. Transdermal delivery is superior to i.h. administration as a route for AAS because it avoids quick clearance of alkaloids and the effect sustains for longer periods. The MN-mediated nanocarrier delivery resulted in superior inhibition of the FCA-induced paw swelling compared to that observed with the two other drug delivery methods.

Histological analysis

No histological changes and infiltration of inflammatory cells were found by histological analysis in normal rats, and the articular cartilage was intact with normal synovial tissue (Figure 5(C)). Sections from the AA model animals displayed notable synovial hyperplasia and massive mononuclear cell infiltration into synovial tissue. The AA rats administered AAS–NLCs by different modes of drug delivery showed a remarkable reduction in the synovial inflammatory cell infiltration and synovial hyperplasia compared with those in the AA rats. In particular, in the group treated with transdermal administration of AAS–NLCs using MNs, there was only a mild inflammatory reaction in the joints of the AA rats. These data also showed that transdermal administration of AAS–NLCs with the use of MNs resulted in a significant decrease of synovial inflammatory cell infiltration and synovial hyperplasia in the AA rats.

Organ index assay

Relative weights of the thymus and spleen, the two major organs of the immune system, are commonly used as preliminary indicators of immunoregulatory activity of drugs [16]. As shown in Figure 5(B), the indexes of the thymus and spleen in the AA group were significantly higher than those in the normal group, whereas no significant impact on the indexes of the heart and kidney was observed in any group ($p > .05$). The results indicated that FCA-induced AA is a systemic inflammation that could induce abnormal swelling of the immune organs. Compared with those in the AA group, both thymus and spleen indexes were markedly ($p < .05$) lower in the patch group, and there was a very significant ($p < .01$) reduction of the indexes of the thymus and spleen in the MN-treated/patch group. A marked reduction was only observed in the index of the spleen when AAS–NLCs were injected subcutaneously. The results suggest that AAS–NLCs

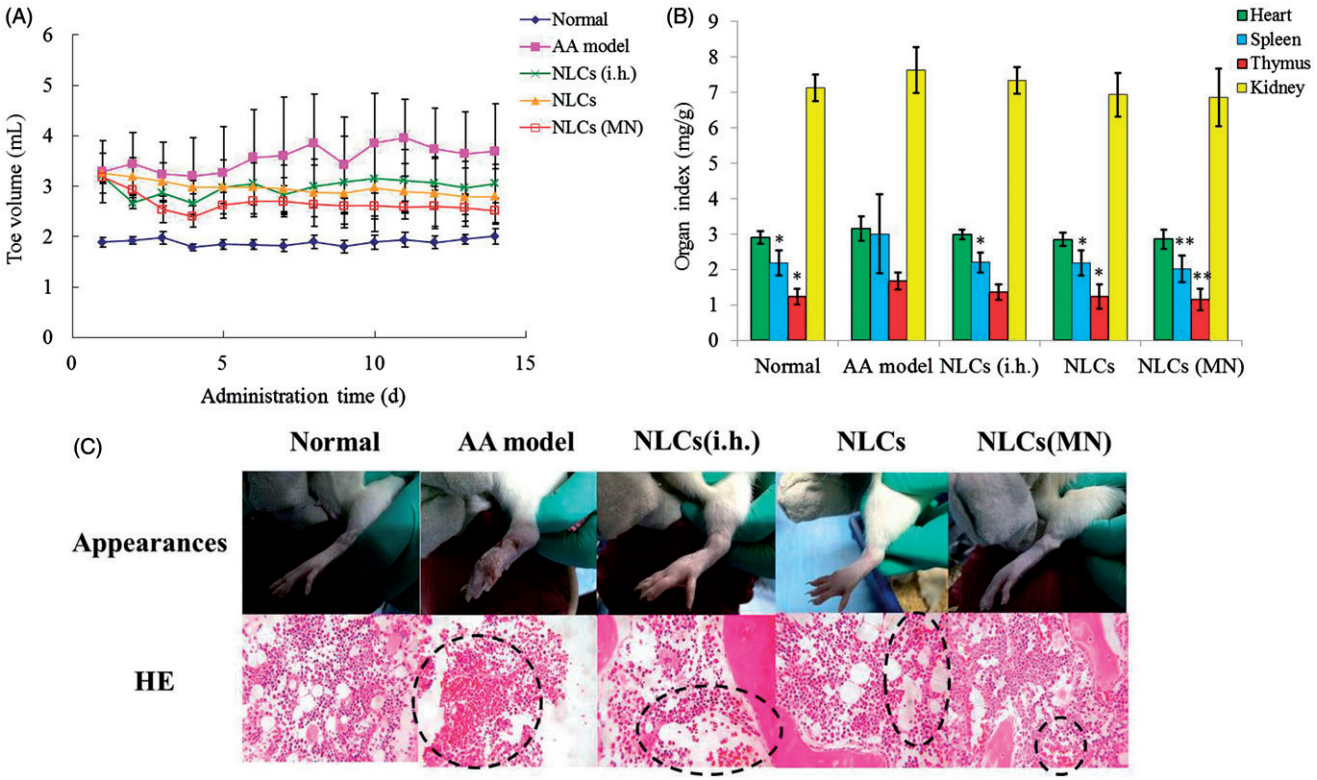

Figure 5. Effects of different administration modes on (A) toe volumes, (B) organ indexes and (C) appearances and histopathological examinations of ankle joints in rats. Inflammatory infiltration areas are marked, $^{**}p < .01$, $^{*}p < .05$ compared with the model group ($n = 8$).

might affect the immune function in the AA rats. Consistent with the superior bioavailability data, the MN-mediated transdermal delivery of nanocarriers for AAS provided the best suppression effect on the abnormal enlargement of immune organs.

Anti-inflammatory and analgesic effects

It has been reported that increased expression of IL-1β, IL-6, and TNFα could increase the expression of other cytokines, stimulate the synthesis of collagen by synovial cells, and lead to cartilage and bone destruction [25,26]. As shown in Figure 6, there was a significant increase in the levels of IL-1β, IL-6, and TNFα in the AA rats compared to those in the normal rats. Both the MN-treated/patch group and patch group showed prominent inhibitory effects on the production of IL-1β, IL-6, and TNFα, while only the TNFα concentration was significantly reduced in the subcutaneous injection group compared to that in the model group. In addition, the reduction in the levels of the cytokines in the MN-treated/patch group was highly significant ($p < .01$). These results show that the MN-mediated transdermal delivery of AAS–NLCs provided the most prominent inhibitory effect on inflammatory cytokines.

The neurotransmitters β-EP, nitric oxide, and SP have been shown to play an important role in the pathophysiology of pain development in animal models and in humans [27–29]. As shown in Figure 6, the concentrations of β-EP and nitric oxide in the serum of the treatment groups were significantly lower, while the level of SP showed no significant difference, compared to those in the model group. These results may be due to the ability of the main components of AAS, including LA, to block the intracellular calcium influx [30].

Skin irritation

As shown in Figure 7, no symptoms of dermal irritation, including an erythema or oedema, were detected on the rabbit skin following the application of NLCs (with or without AAS) and after the MN-mediated AAS–NLC delivery. Moreover, no histopathological changes were identified in the HE-stained paraffin skin sections. This indicated that both AAS–NLCs and the use of MNs to mediate the AAS–NLC delivery had a good biocompatibility with the skin.

Cardiotoxicity

The major analgesic mechanism of the main components of AAS as a calcium channel blocker is blocking the influx of extracellular calcium [29]. On the other hand, an imbalance in intracellular calcium may cause cardiotoxicity such as arrhythmia. Analysis of the rat ECG might provide valuable data about cardiotoxicity, and the utility of rat ECG analysis in toxicology has been claimed [31]. The cardiotoxicity of the drugs delivered via different modes was visualized using ECG (Figure 8). After subcutaneous injection of AAS–NLCs, the rats developed ventricular tachycardia, atrioventricular block, and other serious arrhythmias, as compared with the data obtained for the blank group. These findings are consistent with the results of *in vivo* bioavailability, suggesting that the rapid absorption of alkaloids was the possible cause of the toxicity of subcutaneous injection. The MN-treated/AAS

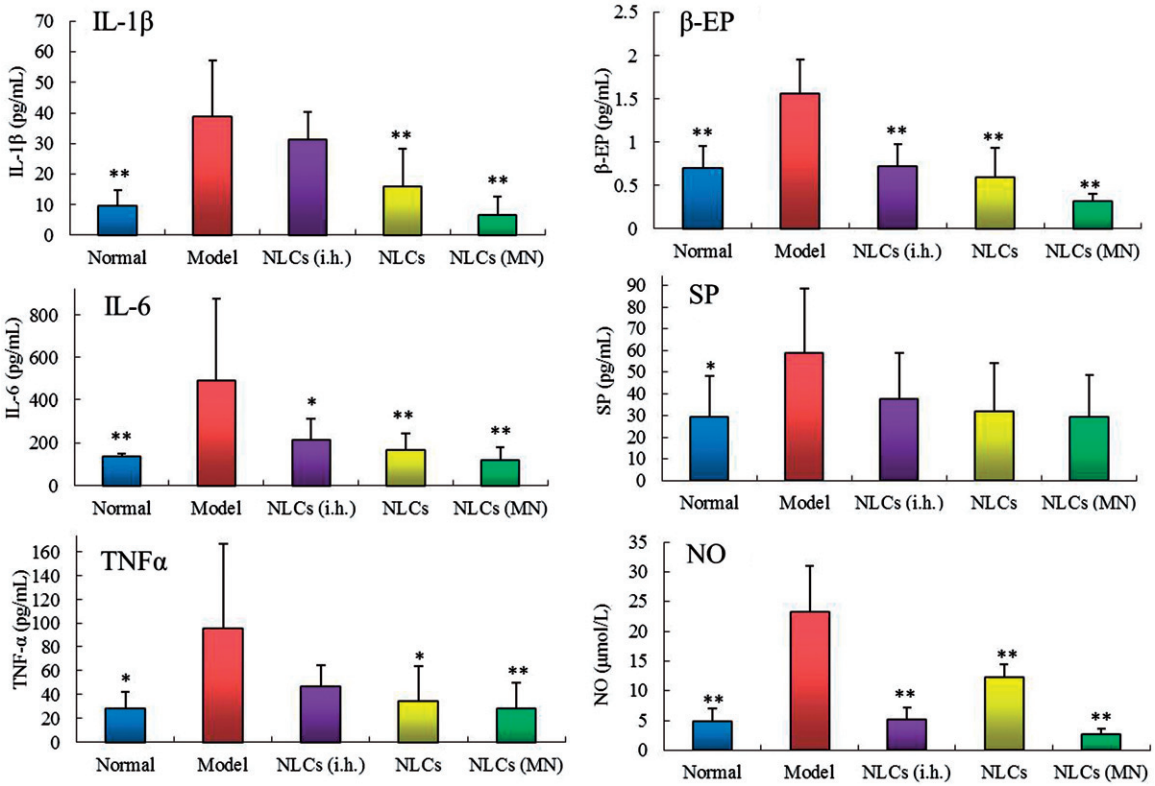

Figure 6. Effects of different treatments on serum levels of inflammatory and pain factors in rats. $^{**}p < .01$, $^{*}p < .05$ compared with the model group ($n = 8$).

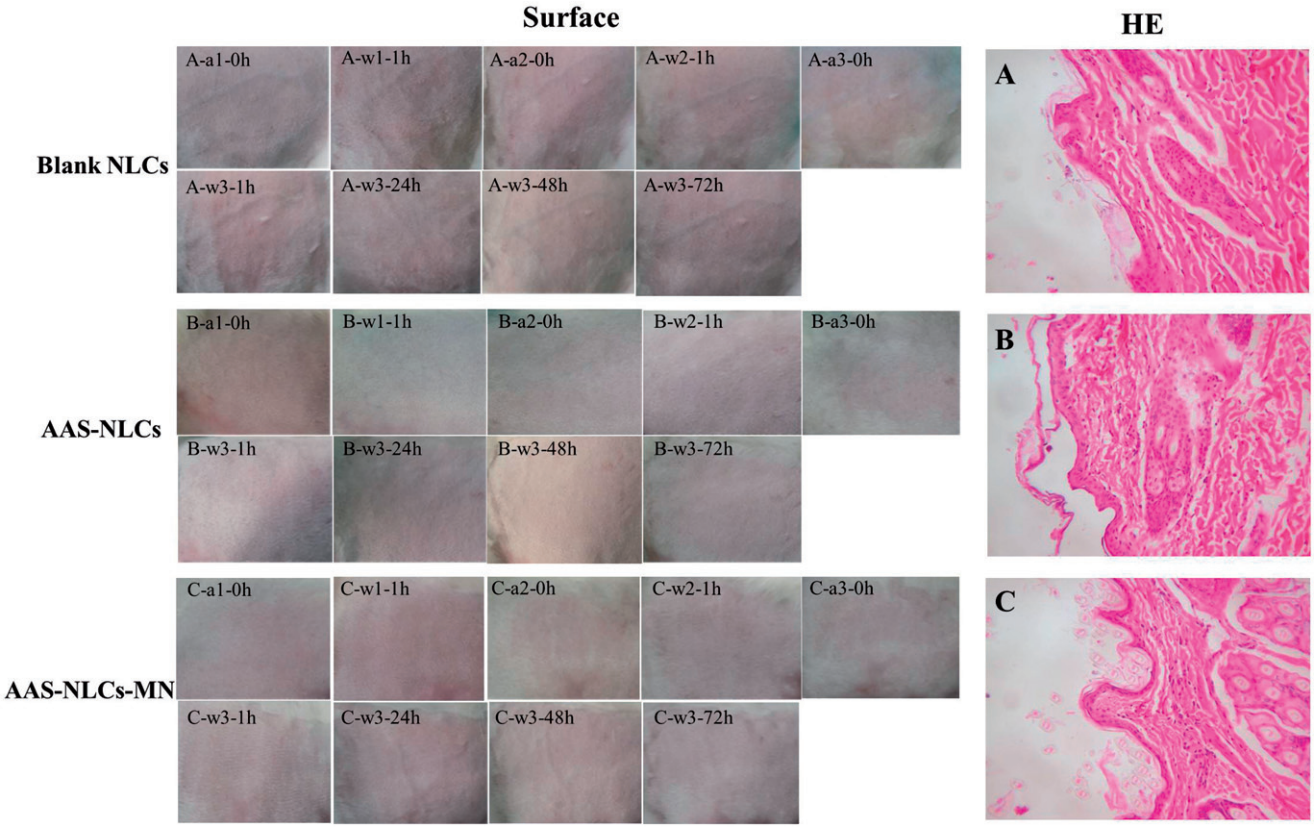

Figure 7. Irritation responses on the surface and microstructure of the rabbit back skin. The skin was treated with (A) blank NLCs; (B) AAS–NLCs; (C) combination of AAS–NLCs and MNs; (a) with drugs applied; (w) with drugs washed off. Magnification: 100×.

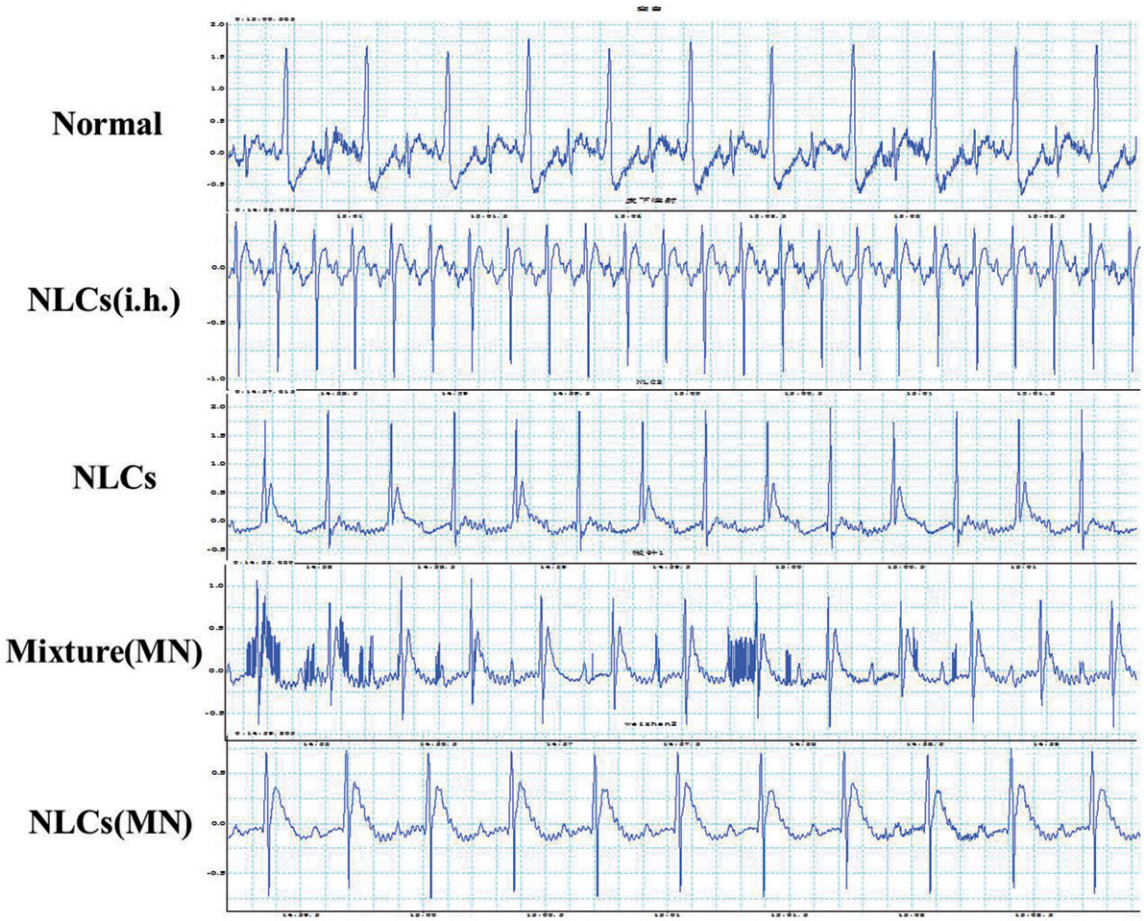

Figure 8. Representative ECG results for rats after percutaneous and hypodermic applications.

mixture patch group revealed a prolonged PR interval and a shortened PP interval, showing a possibility of an atrioventricular block and a right bundle branch block. In comparison, the AAS–NLC patch group and the MN-treated/AAS–NLC patch group merely had a mild atrial block. The results most likely indicate that transdermal delivery could reduce the cardiotoxicity of AAS by maintaining stable blood drug concentrations. Compared with that observed for the MN-mixture delivery, the lower cardiotoxicity of MN–NLC delivery may be attributable to the NLC release through the drug release process.

Conclusions

In this study, the potential of AAS–NLCs combined with MNs for transdermal delivery was investigated. Delivery of AAS–NLCs, driven by MN treatment, resulted in a synergistic effect, which enhanced the penetration of AAS through the skin by combined physical methods (MNs) and chemical methods (NLCs). AAS–NLCs–MN transdermal delivery was used to increase the bioavailability of AAS and maintain the stable drug concentrations in the blood, which could improve the anti-inflammatory and analgesic effects and reduce the cardiotoxicity of AAS. A dual approach involving MN insertion and NLCs can be used to enhance the transdermal delivery of AAS. This will allow optimization of a safe and effective approach for possible transdermal applications of controlled drug delivery systems.

Disclosure statement

No potential conflict of interest was reported by the authors.

Funding

This study was financially supported by a grant (NCET08-0898) from the State Education Ministry of China and the National Natural Science Foundation of China (No. 81573619).

ORCID

Teng Guo http://orcid.org/0000-0002-9213-7068

References

[1] Bhatnagar S, Dave K, Venuganti VVK. Microneedles in the clinic. J Control Release. 2017;260:164–182.

[2] Qiu Y, Gao Y, Hu K, et al. Enhancement of skin permeation of docetaxel: a novel approach combining microneedle and elastic liposomes. J Control Release. 2008;129:144–150.

[3] Shende P, Sardesai M, Gaud RS. Micro to nanoneedles: a trend of modernized transepidermal drug delivery system. Artif Cells Nanomed Biotechnol. 2017. [Epub ahead of print]. doi:10.1080/21691401.2017.1366336.

[4] Vitorino C, Almeida A, Sousa J, et al. Passive and active strategies for transdermal delivery using co-encapsulating nanostructured lipid carriers: in vitro vs. in vivo studies. Eur J Pharm Biopharm. 2014;86:133–144.
[5] Chen J, Wei N, Lopez-Garcia M, et al. Development and evaluation of resveratrol, Vitamin E, and epigallocatechin gallate loaded lipid nanoparticles for skin care applications. Eur J Pharm Biopharm. 2017;117:286–291.
[6] Moghddam SM, Ahad A, Aqil M, et al. Optimization of nanostructured lipid carriers for topical delivery of nimesulide using Box–Behnken design approach. Artif Cells Nanomed Biotechnol. 2017;45:617–624.
[7] Yuan CL, Wang XL. Isolation of active substances and bioactivity of *Aconitum sinomontanum* Nakai. Nat Prod Res. 2012;26:2099–2102.
[8] Guo T, Zhang YT, Zhao JH, et al. Nanostructured lipid carriers for percutaneous administration of alkaloids isolated from *Aconitum sinomontanum*. J Nanobiotechnol. 2015;13:47.
[9] Mak WC, Richter H, Patzelt A, et al. Drug delivery into the skin by degradable particles. Eur J Pharm Biopharm. 2011;79:23–27.
[10] Gomaa YA, Garland MJ, McInnes FJ, et al. Microneedle/nanoencapsulation mediated transdermal delivery: mechanistic insights. Eur J Pharm Biopharm. 2014;86:145–155.
[11] Yin D, Liang W, Xing S, et al. Hepatitis B DNA vaccine-polycation nano-complexes enhancing immune response by percutaneous administration with microneedle. Biol Pharm Bull 2013;36:1283–1291.
[12] Zhang W, Gao J, Zhu Q, et al. Penetration and distribution of PLGA nanoparticles in the human skin treated with microneedles. Int J Pharm. 2010;402:205–212.
[13] Vučen SR, Vuleta G, Crean AM, et al. Improved percutaneous delivery of ketoprofen using combined application of nanocarriers and silicon microneedles. J Pharm Pharmacol. 2013;65:1451–1462.
[14] Zhang YT, Han MQ, Shen LN, et al. Solid lipid nanoparticles formulated for transdermal aconitine administration and evaluated *in vitro* and *in vivo*. J Biomed Nanotechnol. 2015;11:351–361.
[15] Zeb A, Qureshi OS, Yu CH, et al. Enhanced anti-rheumatic activity of methotrexate-entrapped ultradeformable liposomal gel in adjuvant induced arthritis rat model. Int J Pharm. 2017;525:92–100.
[16] Zheng CJ, Zhao XX, Ai HW, et al. Therapeutic effects of standardized *Vitex negundo* seeds extract on complete Freund's adjuvant induced arthritis in rats. Phytomedicine. 2014;21:838–846.
[17] Agrawal U, Gupta M, Vyas SP. Capsaicin delivery into the skin with lipidic nanoparticles for the treatment of psoriasis. Artif Cells Nanomed Biotechnol. 2015;43:33–39.
[18] Lee SG, Jeong JH, Lee KM, et al. Nanostructured lipid carrier-loaded hyaluronic acid microneedles for controlled dermal delivery of a lipophilic molecule. Int J Nanomed. 2014;9:289–299.
[19] Qadri GR, Ahad A, Aqil M, et al. Invasomes of isradipine for enhanced transdermal delivery against hypertension: formulation, characterization, and *in vivo* pharmacodynamic study. Artif Cells Nanomed Biotechnol. 2017;45:139–145.
[20] Lademann J, Richter H, Teichmann A, et al. Nanoparticles-an efficient carrier for drug delivery into the hair follicles. Eur J Pharm Biopharm. 2007;66:159–164.
[21] Gomaa YA, El-Khordagui LK, Garland MJ, et al. Effect of microneedle treatment on the skin permeation of a nanoencapsulated dye. J Pharm Pharmacol. 2012;64:1592–1602.
[22] Wang Q, Li ZJ, Sun L, et al. Pharmacokinetic study of lappaconitine hydrobromide in mice by LC-MS. Yao Xue Xue Bao. 2011;46:432–437.
[23] Panchagnula R, Bokalial R, Sharma P, et al. Transdermal delivery of naloxone: skin permeation, pharmacokinetic, irritancy and stability studies. Int J Pharm. 2005;293:213–223.
[24] Milewski M, Stinchcomb AL. Vehicle composition influence on the microneedle-enhanced transdermal flux of naltrexone hydrochloride. Pharm Res. 2011;28:124–134.
[25] Pearson MJ, Herndler-Brandstetter D, Tariq MA, et al. IL-6 secretion in osteoarthritis patients is mediated by chondrocyte-synovial fibroblast cross-talk and is enhanced by obesity. Sci Rep. 2017;7:3451.
[26] Alam J, Jantan I, Bukhari SNA. Rheumatoid arthritis: recent advances on its etiology, role of cytokines and pharmacotherapy. Biomed Pharmacother. 2017;92:615–633.
[27] Zheng B, Hu L, Song X, et al. Analgesic effect of different moxibustion durations in rheumatoid arthritis rats. J Tradit Chin Med. 2014;34:90–95.
[28] Bredt DS, Snyder SH. Nitric oxide mediates glutamate-linked enhancement of cGMP levels in the cerebellum. Proc Natl Acad Sci USA. 1989;86:9030–9033.
[29] Lisowska B, Siewruk K, Lisowski A. Substance P and acute pain in patients undergoing orthopedic surgery. PLoS One. 2016;11:e0146400.
[30] Guo X, Tang XC. Effects of central Ca^{2+} on analgesic action of lappaconitine. Acta Pharmacol Sin. 1989;10:504–507.
[31] Farraj AK, Hazari MS, Cascio WE. The utility of the small rodent electrocardiogram in toxicology. Toxicol Sci. 2011;121:11–30.